

---

# Crystal: Spontaneous Emergence of Visual Latents in MLLMs

---

Yang Zhang<sup>1\*</sup> Danyang Li<sup>1\*</sup> Yuxuan Li<sup>1†</sup> Xin Zhang<sup>1</sup> Tianyu Xie<sup>2</sup> Mingming Cheng<sup>1</sup> Xiang Li<sup>3,1†</sup>

## Abstract

Multimodal Large Language Models (MLLMs) have achieved remarkable performance by integrating powerful language backbones with large-scale visual encoders. Among these, latent Chain-of-Thought (CoT) methods enable implicit reasoning in continuous hidden states, facilitating seamless vision–language integration and faster inference. However, existing heuristically predefined supervision signals in latent CoT provide limited guidance for preserving critical visual information in intermediate latent states. To address this limitation, we propose Crystal (Crystallized Latent Reasoning), a single-stage framework with two paths to process intact and corrupted images, respectively. By aligning the attention patterns and prediction distributions across the two paths, Crystal crystallizes latent representations into task-relevant visual semantics, without relying on auxiliary annotations or external modules. Extensive experiments on perception-intensive benchmarks demonstrate that Crystal consistently outperforms state-of-the-art baselines, achieving gains in fine-grained visual understanding while maintaining robust reasoning capabilities. Codes are available [here](#).

## 1. Introduction

The rapid evolution of Multimodal Large Language Models (MLLMs) (Liu et al., 2023) has significantly bolstered general-purpose vision-language understanding through the integration of large-scale visual encoders and potent language backbones. By scaling model capacity and diversifying multimodal training corpora, recent systems (Chen et al., 2024; Bai et al., 2025; Wang et al., 2024; Yang et al., 2025a; Zhu et al., 2025) have achieved remarkable performance across a broad spectrum of tasks (Zhang et al.,

2025c; Li et al., 2026; Zhao et al., 2025b;a). To further cultivate complex reasoning, many MLLMs incorporate explicit reasoning mechanisms inspired by Chain-of-Thought (CoT) (Zhang et al., 2023; Shao et al., 2024), which partition intricate queries into intermediate inferential steps.

There are three main paradigms that exist for multimodal CoT, distinguished by their reasoning space. Textual CoT (Xu et al., 2025) converts visual inputs into discrete natural language rationales, while tool-augmented CoT (Zheng et al., 2025) extends this space with dedicated tokens to invoke external modules. In contrast, latent CoT (Chen et al., 2025; Gao et al., 2025; Yang et al., 2025b) performs reasoning directly in continuous hidden states, preserving visual information, avoiding quantization loss, and enabling seamless integration of vision and language. This leads to faster inference and more coherent multimodal reasoning, driving recent advances in interleaved text–image tasks (Su et al., 2025; Zhang et al., 2025a).

Despite these advantages, early latent CoT methods face a limitation: existing supervision signals are often not fully aligned with the nature of latent reasoning. In contrast to textual CoT, where the next-token prediction objective explicitly constrains each intermediate reasoning step, latent CoT relies on supervision that is only indirectly related to the underlying reasoning process. Specifically, the standard next-token loss provides supervision only at the final output level, offering little guidance on how intermediate latent states should encode or preserve critical visual evidence.

To compensate for this mismatch, prior works introduce auxiliary supervision from external vision models such as CoVT (Qin et al., 2025) or human-annotated images such as Monet (Wang et al., 2025a), which is at the price of external modules. However, such signals are heuristic and task-dependent, as they enforce similarity to pre-defined visual features rather than directly supervising reasoning fidelity. Although recent work such as LIVR (Li et al., 2025b) attempts to address this problem via enforcing visual bottlenecks through attention masking, such approaches require multi-stage training pipelines and still cannot guarantee that latent tokens are functionally aligned with the final generation objective. Consequently, such regularization fails to ensure that the latent space maintains semantically grounded visual information. This limitation indicates that the chal-

---

\*Equal contribution <sup>1</sup>VCIP, School of Computer Science, Nankai University <sup>2</sup>Xiamen University <sup>3</sup>Nankai International Advanced Research Institute (Shenzhen Futian). Correspondence to: Yuxuan Li <yuxuan.li.17@ucl.ac.uk>, Xiang Li <xiang.li.implus@nankai.edu.cn>.

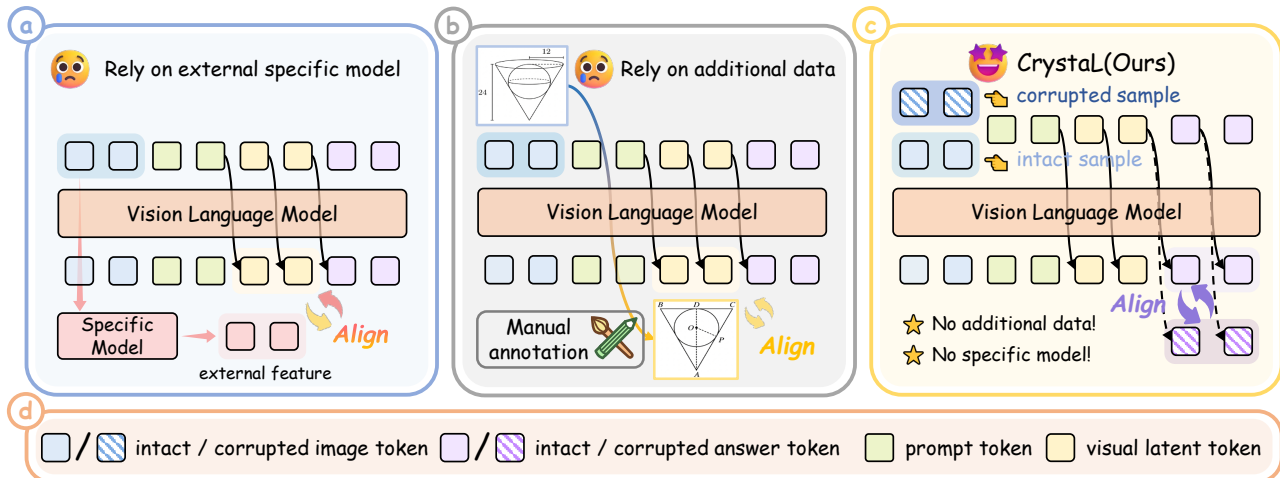


Figure 1. **Previous Paradigms vs. Our Paradigm (Crystal).** (a) describes the paradigm of supervising visual latent tokens via predefined features from specific models, such as SAM (Kirillov et al., 2023), DINO (Caron et al., 2021). (b) denotes the process of modifying original image to guide the reasoning steps. (c) While other methods use auxiliary modules or data to train the visual latent token, CrystalL can do it by self-supervising in a single-stage.

lenge lies not in the absence of supervision, but in the inadequacy of existing supervision paradigms to effectively guide latent reasoning.

In contrast, we propose **CrystalL** (Crystallized Latent Reasoning), a principled *single-stage* framework designed to resolve the misalignment between existing supervision signals and latent reasoning, through a consistency-driven training paradigm. Unlike prior works that necessitate complex multi-stage pipelines, CrystalL employs a dual-path architecture comprising a *intact path* and a *corrupted path*. Specifically, the intact path undergoes standard multimodal training on intact images, while the corrupted path processes visually degraded counterparts. Visual latent representations are copied from the intact path to the corrupted one, enabling the model to recover the ground-truth answer despite the corrupted input. To ensure that these latents are functionally indispensable, we minimize the divergence between the paths’ cross-path attention patterns and output distributions. By enforcing such cross-path consistency, we guide the latent states to “crystallize” into targeted visual semantics which compensate for the corrupted images.

By virtue of this consistency-driven objective, CrystalL encourages latent representations to anchor targeted visual information in a fully self-supervised and task-aligned manner, effectively eliminating the dependence on external priors or manual annotations. Empirical evaluations on perception-intensive benchmarks (including CVBench (Tong et al., 2024), HRBench (Wang et al., 2025b), and VStarBench (Wu & Xie, 2024)) demonstrate that CrystalL yields substantial gains in fine-grained visual understanding while maintaining robust reasoning capabilities. Specifically, CrystalL achieves 76.6% on 2D CVBench, 84.4% on 3D CVBench, 73.4% on 4K HRBench, and 71.1% on 8K HRBench, surpassing

CoVT and LIVR by substantial margins, while also yielding the highest average score (75.4%) across all benchmarks (See Table 2). These results suggest that CrystalL provides a scalable and semantically grounded solution to the long-standing challenge of misalignment between supervision signals and visual latent reasoning. By ensuring that latent inferential steps remain coupled with visual evidence, CrystalL facilitates a more reliable multimodal intelligence.

In summary, this work makes the following contributions:

1. We propose **CrystalL**, a principled single-stage latent CoT framework that guides latent representations to capture task-relevant visual information, enabling efficient and coherent multimodal reasoning.
2. We introduce a dual-path consistency objective that provides task-aligned self-supervision for latent representations, independent of auxiliary annotations or external modules.
3. Extensive experiments demonstrate that CrystalL substantially improves vision-dependent reasoning performance across multiple perception-intensive benchmarks, outperforming strong baselines while maintaining efficient training and inference.

## 2. Related Work

### 2.1. Multimodal Chain-of-Thought Reasoning

Inspired by the success of CoT approaches in pure language models, recent research has focused on endowing MLLMs with similar multi-step reasoning capabilities. Early text-based CoT methods employed prompts to guide models in generating explicit reasoning steps before providing final answers (Zhang et al., 2023; 2025b; Xu et al., 2025). Whilst

effective for scientific Q&A and mathematical problems (Lu et al., 2023), these approaches remain constrained by the limited expressiveness of discrete linguistic symbols when describing continuous visual details. Models tend to rely on self-generated text rather than raw visual inputs, leading to information loss and hallucination phenomena (Wu et al., 2025b; Dong et al., 2025).

To address this, tool-augmented frameworks such as DeepEyes (Zheng et al., 2025) and Visual Programming (Gupta & Kembhavi, 2023) delegate perception tasks to external vision models. However, such pipelines are non-differentiable and heavily reliant on the quality of off-the-shelf tools. Recent hybrid approaches attempt to achieve visually anchored reasoning by interleaving visual features with text (Su et al., 2025), but these typically require costly human annotation of reasoning trajectories or bounding box supervision. In contrast, our proposed Crystal framework cultivates an intrinsic reasoning capability that is fully differentiable and self-supervised, eliminating reliance on external tools or dense annotations.

### 2.2. Latent Space Reasoning

Moving beyond explicit text generation, research focus has shifted towards latent reasoning, wherein the inferential process unfolds within a sequence of hidden states. Within the realm of pure language models, Coconut (Hao et al., 2024) and Quiet-STaR (Zelikman et al., 2024) demonstrate that models can engage in ‘thinking’ through implicit vectors prior to generating output responses, without requiring verbose textual expressions. This paradigm is now extending to multimodal large language models. For instance, MintCoT (Chen et al., 2025) establishes a mapping between patch indices and visual tokens to provide direct supervision. Monet introduces a specialized dataset featuring images that describe reasoning trajectories, supervising intermediate steps by aligning token features with dataset images. Similarly, CoVT (Qin et al., 2025) leverages external visual models to supervise the latent features of visual tokens. However, these approaches rely on generic language modeling objectives (next-token prediction) and do not explicitly penalise the utility of visual information within reasoning. In contrast, our work distinguishes itself by introducing a visual consistency objective, explicitly compelling implicit inference chains to preserve targeted visual semantics even when inputs are corrupted.

### 2.3. Self-Supervised Visual Representation Learning

Our training paradigm draws inspiration from the success of self-supervised learning in computer vision. Masked image modeling (He et al., 2022) and contrastive learning (Chen et al., 2020; Grill et al., 2020) demonstrate that robust visual representations can be learned by either reconstructing

Table 1. Key properties of visual latent reasoning methods. In contrast to prior works like Aurora (Bigverdi et al., 2025), SKILA (Tong et al., 2025), LVR (Li et al., 2025a), LIVR, and CoVT, our Crystal is the only framework that simultaneously satisfies all criteria. Specifically, it eliminates the need for auxiliary modules and supplementary image labels while enabling efficient one-stage training. Symbols in green denote desired properties, while those in red denote undesired ones.

Desired Properties	Aurora	SKILA	LVR	LIVR	CoVT	Ours
No extra module	✗	✗	✓	✓	✗	✓
No extra images needed for training	✓	✗	✓	✓	✓	✓
One-stage training	✗	✓	✗	✗	✗	✓
Reason in the continuous space	✗	✓	✓	✓	✓	✓

corrupted inputs. While these methods are originally designed for pretraining conventional encoders, recent studies on multimodal large language models began applying these principles during post-training alignment (Li et al., 2025c). For instance, visual Jigsaw (Wu et al., 2025a) enhances fine-grained perception through a jigsaw puzzle task, and CapPO (Tu et al., 2025) reduces hallucination via caption consistency. However, these approaches typically operate at the output level. In contrast, Crystal applies consistency regularization directly within the latent reasoning space, requiring that implicit states derived from intact images effectively restore the model’s reasoning capability on corrupted inputs—thus grounding reasoning firmly in visual content.

## 3. Method

We propose Crystal, a single-stage dual-path framework that instills robust latent reasoning into MLLMs via Latent Crystallization, which anchors targeted semantics into dedicated latent tokens. We first introduce the chain of thought reasoning in Sec. 3.1. We then introduce Stochastic Image Corruption (SIC) in Sec. 3.2. Next we describe the dual-path framework used to enforce latent-level dependencies in Sec. 3.3. Finally we formulate the objective of optimization in Sec. 3.4 and Sec. 3.5

### 3.1. Reasoning with Chain of Thoughts

In the context of Multimodal Large Language Models (MLLMs), let  $\mathcal{M}$  denote the model. Given a visual input  $I$  and a textual query  $Q$ , the model generates an output sequence  $Y = \{Y_0, Y_1, \dots, Y_n\}$  token by token. The generation process is formulated as:

$$P_{\mathcal{M}}(Y|I, Q) = \prod_i P_{\mathcal{M}}(Y_i|Y_{<i}, I, Q), \quad (1)$$

where  $Y_{<i}$  represents the sequence of tokens predicted prior to step  $i$ . In standard Fine-tuning for Visual Question Answering (VQA), the objective is to maximize the likelihood of the ground-truth answer  $P_{\mathcal{M}}(Ans|I, Q)$ .

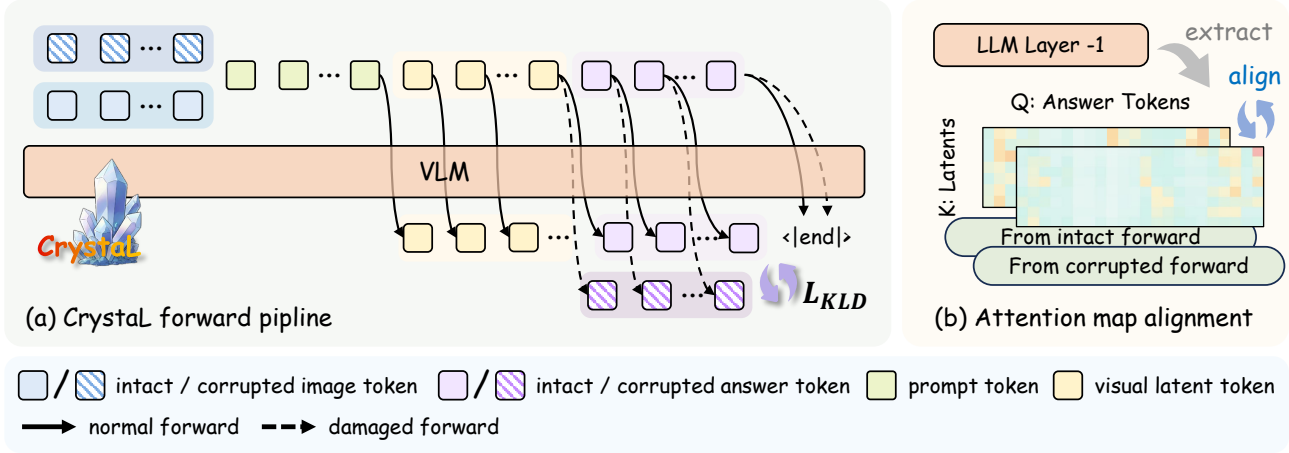


Figure 2. **An overview of CrystalL.** (a) Starting by corrupting the raw image, we construct two types of visual tokens from vision encoder. Then both the  $S_{int}$  and  $S_{cor}$  in Sec. 3.3 are fed into the model to compute the  $P_{int}$  and  $P_{cor}$ . But the hidden states of corrupt forward (dashed arrow) indeed come from the intact forward (solid arrow). For the objective function, we adopt a combination of cross entropy loss and alignment loss, the attention map alignment is illustrated in (b).

To enhance the model’s complex reasoning capabilities, we incorporate the Chain-of-Thought (CoT) paradigm. Under this setting, the objective function is based on a joint probability distribution:

$$P_{\mathcal{M}}(Ans, CoT|I, Q), \quad (2)$$

where  $CoT$  represents a sequence of intermediate reasoning steps. The introduction of  $CoT$  effectively decomposes the complex mapping from visual-textual inputs to the final answer, allowing the model to allocate more computational steps to internal logic before arriving at a conclusion.

While conventional CoT sequences consist of discrete textual tokens, the concept of **Latent CoT** has been proposed. In this formulation, reasoning steps are represented as continuous latent variables within the model’s hidden space. Our framework primarily supervises the representations in the latent space during training to preserve high-dimensional semantic nuances that discrete tokens might fail to capture.

### 3.2. Visual Corruption as Information Bottleneck

A fundamental challenge in training latent reasoning models is to ensure the visual latent tokens used, since raw visual tokens often contain sufficient cues for the model to answer the question, it tends to skip these latent reasoning paths. This implicitly hinders the emergence of genuine visual latent reasoning, as the model arrives at answers without effectively engaging the continuous hidden states. To address this, we introduce the **Stochastic Image Corruption (SIC)** module. SIC acts as a generalized operator  $\mathcal{C}$  that maps the high-fidelity image  $I$  into a degraded observation  $I_{cor}$ :

$$I_{cor} = \mathcal{C}(I; \eta, \mathcal{S}), \quad \eta \sim p(H), \quad (3)$$

where  $\mathcal{S}$  denotes the corruption mode and  $\eta$  is the stochastic intensity sampled from a prior distribution  $p(H)$ . To explore the resilience of latent reasoning, we consider a diverse library of corruption primitives  $\mathcal{S} \in \{\mathcal{G}, \mathcal{K}, \mathcal{V}, \mathcal{N}\}$ :

- **Spectral Decay ( $\mathcal{G}$ ):** Gaussian-based low-pass filtering that suppresses high-frequency textures while preserving global topology.
- **Spatial Discontinuity ( $\mathcal{K}$ ):** Random cropping, masking, or Jigsaw shuffling that disrupts the geometric coherence of visual evidence.
- **Chromatic Distortion ( $\mathcal{V}$ ):** Jittering color distributions to isolate semantic shape from pixel-level intensity by decoupling invariant structural geometry from transient global photometric fluctuations.
- **Stochastic Noise ( $\mathcal{N}$ ):** Additive Gaussian or impulse noise to the input tensors.

### 3.3. Dual-Path Latent Reasoning Framework

The model processes the multimodal query through two parallel streams illustrated in Fig. 2. During training, the **causal attention mechanism** allows the computation of output logits for the entire sequence in a single forward pass. Specifically, for an input containing an image  $I$  and text sequence  $text = \{t_1, t_2, \dots, t_L\}$  of length  $L$ , the model  $\mathcal{M}$  can generate a sequence of hidden states  $\mathbf{H} = \{h_1, \dots, h_L\}$ , which are subsequently mapped to the predicted probability distributions (logits) over the vocabulary  $\mathcal{V}$  at each position. So in the training stage the labels directly come from the shifted sequence. As we add several pad tokens to shape the  $CoT = \{intermediate\ steps, < visual\ tokens \}$ ,

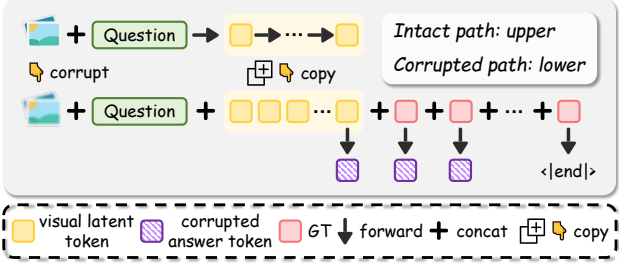


Figure 3. **Detailed illustration of visual latent token copying.** For the forward process, the autoregressive hidden states of visual latent tokens in the corrupted path is copied from the intact path.

the sequence is like  $\{I, Q, CoT, Ans\}$ , where  $Ans$  is the ground-truth answer. Then we process the sequence in the dual-path framework.

**The Intact Path.** This path receives the high-fidelity image  $I_{int} = I$ . The input sequence is formulated as  $S_{int} = \{I_{int}, Q, CoT, Ans\}$ . As the “teacher” stream, it leverages complete visual evidence to compute the latent states value of visual tokens  $\mathbf{T}_{lat} = \{T_1, T_2, \dots, T_l\}$  ( $l$  represents the number of layers of the language model) to provide the raw information of an intact sample such that the corrupted path will borrow the latents to conduct the “crystalization” operation. And the intact path naturally generates the logits  $\mathbf{P}_{int}$  for the computation of cross entropy loss and work as a reference of the corrupted path.

**The Corrupted Path.** This path operates on the perturbed image  $I_{cor} = \mathcal{C}(I)$ . The corresponding input sequence  $S_{cor} = \{I_{cor}, Q, CoT, Ans\}$ . We enforce a **latent-level dependency** by replacing the latent representations at each decoder layers in the corrupted path with corresponding latents in  $\mathbf{T}_{lat}$  derived from the intact path. The model then generates the logits  $\mathbf{P}_{cor}$  for the perturbed sequence.

By constructing the dual-path framework, we bypass the difficulty of labeling data by hand to supervise the visual tokens. Because the  $\mathbf{T}_{lat}$  with complementary information from intact path will facilitate the corrupted path, which enforce the visual tokens to work as indispensable ingredient of reasoning. The supervision from the next token loss will naturally work on the visual tokens.

### 3.4. Alignment Objectives

As the above dual-path framework constructs the base of “crystalization”, the hidden states  $\mathbf{T}_{lat}$  has been copied from the intact path to the corrupted path. Then we need to supervise the model to motivate the  $\mathbf{T}_{lat}$  to absorb the robust feature of the image.

**Predictive Distribution Consistency ( $\mathcal{L}_{kl}$ ).** To effectively anchor the reasoning process within the latent space,

we supervise the corrupted path using the high-fidelity outputs of the intact path as a reference. This is achieved through a consistency-driven alignment objective applied to the predictive distributions.

Specifically, the objective is to conduct a logit-level loss between  $\mathbf{P}_{int}$  and  $\mathbf{P}_{cor}$ , targeting at the tokens corresponding to the ground-truth  $Ans$ . This targeted alignment compels the latent reasoning states to “crystallize” into targeted visual representations that are functionally indispensable for the final generative process.

To ensure that the model maintains robust decision-making despite visual degradation, we minimize the Kullback-Leibler (KL) divergence between the output probability distributions of the two paths. Specifically, this loss is calculated over the tokens corresponding to the ground-truth answer  $A = \{a_1, \dots, a_M\}$ , forcing the corrupted path to emulate the predictive confidence of the intact path:

$$\mathcal{L}_{kl} = \frac{1}{M} \sum_{i \in \Omega_A} D_{KL}(\mathcal{P}(\hat{y}_i | S_{int}) \parallel \mathcal{P}(\hat{y}_i | S_{cor})), \quad (4)$$

where  $\Omega_A$  denotes the set of indices for the answer tokens, and  $\mathcal{P}(\hat{y}_i | \cdot)$  represents the predicted probability distribution over the vocabulary  $\mathcal{V}$  at the  $i$ -th position. By optimizing this objective, we compel the model to recover the targeted semantics from the transferred latent tokens  $\mathbf{T}_{lat}$ , bridging the gap caused by the input corruption.

**Mechanistic Consistency ( $\mathcal{L}_{attn}$ ).** While predictive consistency aligns the final outputs, it does not inherently guarantee that both path follow the same inferential pattern. We then enforce consistency within the internal attention mechanism. Specifically, we constrain the attention weights assigned by the answer tokens to the visual latent tokens. Let  $\mathbf{A} \in \mathbb{R}^{H \times M \times K}$  denote the aggregated attention maps across  $H$  heads, representing the attention scores from  $M$  answer tokens to  $K$  latent tokens. We minimize the squared Frobenius norm of the discrepancy between the two paths:

$$\mathcal{L}_{attn} = \mathbb{E}_{l \in \mathcal{L}_{sub}} \left\| \mathbf{A}_{int}^{(l)} - \mathbf{A}_{cor}^{(l)} \right\|_F^2, \quad (5)$$

where  $\mathcal{L}_{sub}$  represents a selected subset of decoder layers. By optimizing  $\mathcal{L}_{attn}$ , we ensure that even when fine-grained visual details are neutralized, the model’s reasoning behavior—reflected in its localized attention over the latent space—remains stable and firmly grounded in the semantic representations encoded by the visual latent tokens distilled from the original image.

### 3.5. Overall Training Objective

To facilitate latent crystallization while preserving the fundamental instruction-following and generative capabilities

Table 2. Comparison of model performance across diverse visual benchmarks. The results highlight Crystal’s superior capabilities comparing with baselines including Qwen2.5-VL-7B (Bai et al., 2025).

Method	CVBench		HRBench		BLINK	RWQA	V*	POPE	Average
	2D	3D	4K	8K					
<b>Closed-source Methods</b>									
Claude-4-Sonnet	-	-	32.3	22.7	39.6	63.7	15.2	-	-
GPT-4o	-	-	50.6	46.7	63.0	69.7	42.9	-	-
<b>Open-source Methods</b>									
Qwen2.5-VL-7B	75.0	73.3	68.6	64.9	55.7	68.6	76.4	86.5	71.1
CoVT (Qin et al., 2025)	<u>75.1</u>	<b>84.7</b>	71.0	<u>69.4</u>	<u>56.0</u>	<b>71.6</b>	78.0	84.6	73.8
LVR (Li et al., 2025a)	-	-	69.6	66.1	52.5	67.7	81.7	-	-
Vision-R1 (Huang et al., 2025)	8.0	37.6	64.8	57.0	51.0	9.4	80.1	77.8	48.2
LIVR (Li et al., 2025b)	73.9	82.7	<u>72.4</u>	69.0	56.3	69.2	79.1	<b>89.5</b>	<u>74.0</u>
SKILA (Tong et al., 2025)	-	-	72.0	66.5	<b>56.7</b>	70.5	<b>84.3</b>	87.3	-
<b>Our Method</b>									
<b>Crystal</b>	<b>76.6</b>	<u>84.4</u>	<b>73.4</b>	<b>71.1</b>	55.9	<u>70.6</u>	<u>82.7</u>	<u>88.7</u>	<b>75.4</b>
$\Delta$ (vs Qwen2.5-VL-7B)	<b>+1.6</b>	<b>+11.1</b>	<b>+4.8</b>	<b>+6.2</b>	<b>+0.2</b>	<b>+2.0</b>	<b>+6.3</b>	<b>+2.2</b>	<b>+4.3</b>

of the MLLM, we integrate the proposed alignment objectives with the cross entropy loss into a unified *single-stage* optimization framework.

**Cross Entropy Loss  $\mathcal{L}_{ce}^{int}$  and  $\mathcal{L}_{ce}^{cor}$ .** A cross-entropy loss on the corrupted path, denoted as  $\mathcal{L}_{ce}^{cor}$ , encourages the model to seek information from the visual latent tokens when the visual input is corrupted and thus unavailable, thereby enabling the latent representations to encode meaningful visual information. In order to keep the model output the sequence in the format of standard chain of thought, a cross entropy loss in the intact path  $\mathcal{L}_{ce}^{int}$  is also introduced.  $\mathcal{L}_{ce}^{int}$  will then enforce the model make use of the visual latent tokens to keep reasoning ability in the vanilla mode where the image is intact.

The total training loss is formulated as a combination of the generative and consistency-driven terms:

$$\mathcal{L}_{total} = \mathcal{L}_{ce}^{int} + \mathcal{L}_{ce}^{cor} + \mathcal{L}_{kl} + \mathcal{L}_{attn}, \quad (6)$$

where  $\mathcal{L}_{ce}^{int}$  and  $\mathcal{L}_{ce}^{cor}$  denote the standard next-token prediction losses (cross-entropy) computed on the intact and corrupted paths, respectively.

Under this unified formulation, the model is incentivized not only to generate coherent textual responses but also to *actively* encode task-essential visual semantics into the specialized latent tokens  $\mathbf{T}_{lat}$ . As a result,  $\mathbf{T}_{lat}$  functions as a repository of **semantic invariants** that capture high-level visual evidence capable of sustaining complex reasoning even under severely degraded perceptual conditions. This objective ensures the emergence of a latent reasoning path that is both **consistent across diverse visual views** and **deeply grounded** in the underlying visual logic, providing a scalable solution to the challenge of misalignment between supervision signals and visual latent CoT.

## 4. Experiment

### 4.1. Experimental Setup

**Training Configurations** We fine-tune our model using LoRA (Hu et al., 2022) with a rank  $r = 16$  and an alpha  $\alpha = 32$ . The learning rates are set to  $2 \times 10^{-4}$  for LoRA adapters. All experiments are conducted on a workstation equipped with  $4 \times$  NVIDIA A40 GPUs.

**Benchmarks.** We evaluate all models using VLMEvalKit (Duan et al., 2024), a standardized evaluation framework for multimodal large language models. To comprehensively assess the visual perception and reasoning capabilities of Crystal, we conduct experiments across multiple representative benchmarks covering complementary evaluation aspects. We adopt RealWorldQA (RWQA) (Zhang et al., 2024), BLINK (Fu et al., 2024), V\*Bench (V\*) (Wu & Xie, 2024), and HRBench (HR4K and HR8K) (Wang et al., 2025b). These benchmarks focus on fine-grained visual understanding, compositional reasoning, and high-resolution image comprehension, encompassing challenging real-world scenarios such as complex visual layouts and detailed spatial relations. To further examine the robustness of Crystal against multimodal hallucination, we evaluate our model on POPE (Li et al., 2023), which is specifically designed to diagnose hallucinated visual claims in MLLMs.

**Baselines.** We compare Crystal with several representative methods that explore latent or explicit reasoning in multimodal models. **LVR** is a two-stage framework that performs supervised fine-tuning followed by reinforcement learning to induce latent visual reasoning. **SKILA** introduces a sketch-in-latent paradigm, aiming to elicit unified

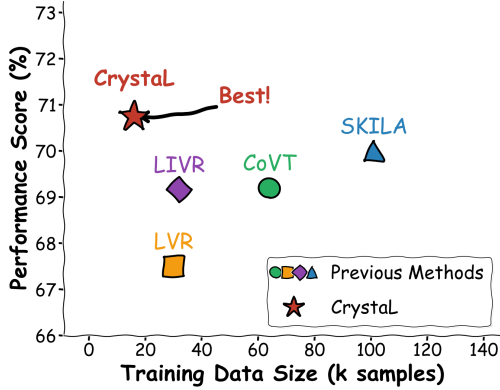


Figure 4. Comparison of performance and training data size. Our method achieves superior performance while utilizing significantly fewer samples than baselines, demonstrating exceptional data efficiency.

multimodal reasoning by encoding structured visual abstractions into latent representations. LIVR constructs an implicit visual bottleneck via non-causal attention masking, encouraging the model to rely on latent visual cues rather than direct pixel-level features. Vision-R1 (Huang et al., 2025) enhances multimodal reasoning ability through a combination of supervised fine-tuning and reinforcement learning, focusing on reasoning behavior rather than directly supervising by visual grounding.

## 4.2. Quantitative analysis

Comprehensive results are summarized in Table 2, where the data reveals that CrystalL sets a new state-of-the-art across most benchmarks, achieving a leading average score of 75.4%. Specifically, CrystalL demonstrates a significant advantage in high-resolution perception, outperforming the baseline Qwen2.5vl by 4.8% and 6.2% on the challenging HRBench 4K and 8K tracks.

Furthermore, while models like LIVR and SKILA show competitive results in specific hallucination or video benchmarks (e.g., POPE and VStarBench), CrystalL maintains the most balanced performance profile. The comparative degradation of Vision-R1 in CVBench-2D and RWQA highlights the robustness of our architectural design in maintaining multimodal reasoning consistency.

**Data Efficiency.** We evaluate the training efficiency of our framework by comparing the performance against various baselines on the intersection of benchmarks, including BLINK, HRBench, RealWorld-QA, and VStarBench. As illustrated in Fig. 4, our method achieves a state-of-the-art accuracy using only 16k training samples. Notably, this outperforms SKILA, which requires 100k samples. This comparison highlights that our latent reasoning mechanism enables the model to achieve superior multimodal understanding with over  $6\times$  fewer data, demonstrating a signifi-

Table 3. Ablation on the quantity and content of latent reasoning tokens. The upper section denotes configurations using same tokens, while the lower section utilizes diverse tokens.

Quantity	CV <sub>2D</sub>	CV <sub>3D</sub>	BLINK	HR <sub>4K</sub>	HR <sub>8K</sub>	RWQA	Avg
Baseline							
Qwen2.5-VL	75.0	73.3	55.7	68.6	64.9	68.6	67.7
Identical latent token							
4 tokens	74.7	74.7	52.9	73.8	71.0	68.0	69.2
8 tokens	75.7	83.7	54.4	<b>74.4</b>	<b>72.0</b>	69.3	71.6
16 tokens	72.3	80.6	52.3	71.5	68.1	69.7	69.1
Diverse latent token							
4 tokens	75.1	82.9	55.3	73.8	70.8	69.8	71.3
8 tokens	<b>76.6</b>	<b>84.4</b>	<b>55.9</b>	73.4	71.1	70.6	<b>72.0</b>
16 tokens	74.0	72.6	53.9	74.3	71.4	<b>71.6</b>	69.6

Table 4. Ablation on alignment strategy. Both the  $\mathcal{L}_{kl}$  and  $\mathcal{L}_{attn}$  play a critical role in our method. And the type of  $\mathcal{L}_{attn}$  is also important. Here, “Cor.” means “corrupted”.

Strategy	CV <sub>2D</sub>	CV <sub>3D</sub>	BLINK	HR <sub>4K</sub>	HR <sub>8K</sub>	RWQA	Avg
How does the intact path assist corrupted path?							
Qwen2.5-VL	75.0	73.3	55.7	68.6	64.9	68.6	67.7
+ Cor. CE	74.7	83.3	54.6	73.0	70.3	69.9	71.0
+ Cor. CE + KL	75.2	83.6	54.1	<b>75.0</b>	71.1	<b>71.1</b>	71.7
+ Cor. CE + Att. Align	76.2	84.0	<b>57.1</b>	72.6	70.4	70.3	71.8
+ All	<b>76.6</b>	<b>84.4</b>	55.9	73.4	<b>71.1</b>	70.6	<b>72.0</b>
Attention map alignment strategy							
Answer to All (KL)	73.6	79.5	53.9	74.8	69.4	69.5	70.1
Answer to Latents (KL)	<b>76.6</b>	<b>84.4</b>	<b>55.9</b>	73.4	71.1	<b>70.6</b>	<b>72.0</b>
Answer to Latents (MSE)	76.3	83.1	54.0	<b>73.8</b>	<b>71.4</b>	70.2	71.4

cant advantage in data-scarce scenarios.

## 4.3. Ablation Study

**Ablation on token numbers and type.** This section provides a detailed analysis that elucidates the impact of latent token configurations on the overall capacity of CrystalL. As Table 3 shows, our results reveal two key insights: first, employing diverse tokens consistently outperforms the use of identical tokens, a finding which underscores that semantic variety in the latent space is crucial for capturing complex multimodal dependencies. Second, we observe a non-monotonic relationship between performance and token count, where a length of 8 tokens achieves the optimal balance, surpassing both shorter (4) and longer (16) sequences in both settings.

**Ablation on alignment strategy.** To demonstrate the effectiveness of our alignment strategy, we conduct an ablation study on the loss functions. As shown in Table 4, the model yields the lowest performance when optimized solely with cross-entropy loss. Incorporating KL-loss or Alignment-loss into the objective consistently improves results, with the performance reaching its peak when all components are combined in the Full configuration.

Table 5. **Ablation on corruption strategy.** The Gaussian blur behaves best in all the corruption strategies, while random mask is also useful for learning visual latents.

Strategy	CV <sub>2D</sub>	CV <sub>3D</sub>	BLINK	HR <sub>4K</sub>	HR <sub>8K</sub>	RWQA	Avg
Gaussian Blur	76.6	84.4	55.9	73.4	71.1	70.6	72.0
Random Mask	76.3	84.7	55.2	71.9	69.4	68.4	71.0
Jigsaw Shuffling	73.6	82.5	54.0	71.4	69.0	65.2	69.3
Gaussian Noise	74.9	81.8	54.1	72.0	69.8	69.9	70.4
Colour Distortion	74.8	80.3	54.6	72.3	70.4	70.6	70.5

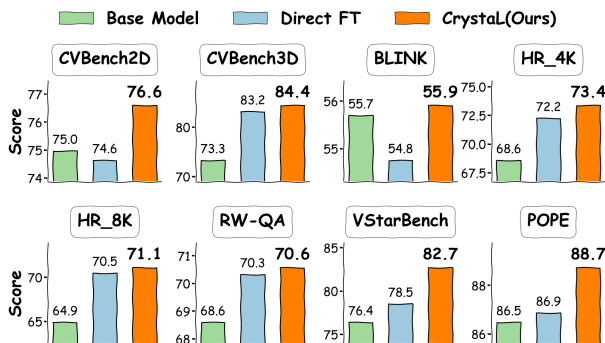


Figure 5. **Direct Finetune vs Crystal.** CrystalL outperforms direct finetuning’s capabilities across all the tasks.

Furthermore, we investigate how the specific formulation of alignment affects model performance. While adopting a standard MSE-based alignment provides marginal gains, it lacks the flexibility to capture complex cross-modal dependencies. Notably, we found that applying KL-type alignment to the entire attention map (from answer to both image and latent tokens) actually degrades performance. The model achieves its best performance only when the alignment is restricted to the attention from answer tokens (as queries) to latent tokens (as keys).

**Ablation on corruption strategy.** We evaluate different corruption strategies  $\mathcal{C}$  in the proposed SIC module, including Gaussian blur, random masking, colour distortion, jigsaw shuffling, additive Gaussian noise. As shown in Table 5, Gaussian blur consistently achieves the best performance across all benchmarks, while other corruption types lead to inferior results.

We hypothesize that spatial perturbations (e.g., jigsaw or random masking) often introduce artificial edge artifacts that lead to a distribution shift in the visual encoder’s feature map, potentially hindering the model’s basic recognition. But Gaussian blur strikes the best balance between information suppression and semantic preservation, making it the most suitable corruption strategy in our framework. Consequently, we adopt Gaussian-based corruption as the default setting in other experiments.

**Ablation on direct finetune** To isolate the contribution of our latent reasoning mechanism, we conduct an ablation

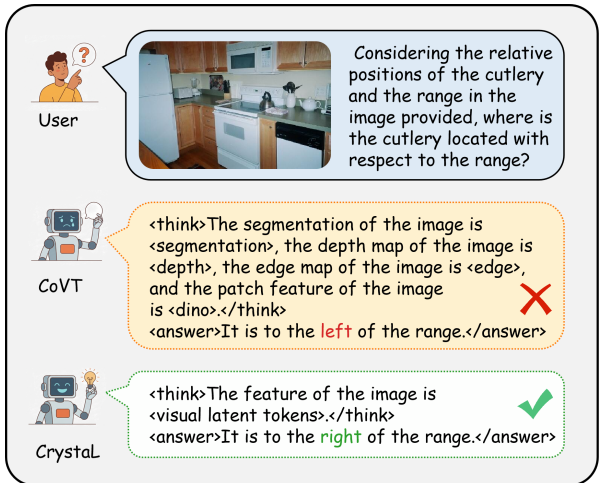


Figure 6. **Qualitative comparison on CVBench-2D.** We illustrate the responses from CoVT and CrystalL to a question regarding spatial-relational reasoning between objects.

study comparing CrystalL with a direct fine-tuning (Direct FT) baseline. As shown in Fig. 5, although Direct FT improves upon the base model, it consistently underperforms compared to CrystalL across all eight benchmarks. Specifically, in perception-intensive tasks such as CVBench2D and VStarBench, CrystalL achieves absolute gains of 2.7% and 4.2% over Direct FT, respectively. This performance gap demonstrates that simply updating model weights via standard supervised fine-tuning is insufficient for complex multimodal tasks. Instead, our latent thinking process provides a more effective pathway for the model to internalize and utilize dense visual evidence for inference.

#### 4.4. Qualitative Analysis

To demonstrate the enhanced perceptual capabilities afforded by our CrystalL framework, we present a case study from the CVBench-2D dataset where CrystalL outperforms CoVT as Fig. 6 shows. Notably, even with the integration of SAM, DINO, Depth Anything (Yang et al., 2024) for structural alignment, CoVT struggles in relations between objects while CrystalL yields the correct answer.

### 5. Conclusion

In this paper, we introduced CrystalL, a novel single-stage training framework for visual latent reasoning. By employing a dual-path architecture, CrystalL enables visual latent tokens to be naturally supervised without relying on external modules or auxiliary images. Our experimental results demonstrate that CrystalL not only achieves superior performance across various benchmarks but also establishes a more efficient paradigm for visual reasoning. This work provides a scalable and streamlined approach for the development of multimodal large language models.

## Impact Statement

This paper presents work whose goal is to advance the field of Machine Learning. There are many potential societal consequences of our work, none which we feel must be specifically highlighted here.

## References

- Acharya, M., Kafle, K., and Kanan, C. Tallyqa: Answering complex counting questions. In *Proceedings of the AAAI conference on artificial intelligence*, pp. 8076–8084, 2019.
- Bai, S., Chen, K., Liu, X., Wang, J., Ge, W., Song, S., Dang, K., Wang, P., Wang, S., Tang, J., et al. Qwen2. 5-vl technical report. *arXiv preprint arXiv:2502.13923*, 2025.
- Bigverdi, M., Luo, Z., Hsieh, C.-Y., Shen, E., Chen, D., Shapiro, L. G., and Krishna, R. Perception tokens enhance visual reasoning in multimodal language models. In *Proceedings of the Computer Vision and Pattern Recognition Conference*, pp. 3836–3845, 2025.
- Caron, M., Touvron, H., Misra, I., Jégou, H., Mairal, J., Bojanowski, P., and Joulin, A. Emerging properties in self-supervised vision transformers. In *Proceedings of the IEEE/CVF international conference on computer vision*, pp. 9650–9660, 2021.
- Chen, T., Kornblith, S., Norouzi, M., and Hinton, G. A simple framework for contrastive learning of visual representations. In *International conference on machine learning*, pp. 1597–1607. PmLR, 2020.
- Chen, X., Zhang, R., Jiang, D., Zhou, A., Yan, S., Lin, W., and Li, H. Mint-cot: Enabling interleaved visual tokens in mathematical chain-of-thought reasoning. *arXiv preprint arXiv:2506.05331*, 2025.
- Chen, Z., Wu, J., Wang, W., Su, W., Chen, G., Xing, S., Zhong, M., Zhang, Q., Zhu, X., Lu, L., et al. Internvl: Scaling up vision foundation models and aligning for generic visual-linguistic tasks. In *Proceedings of the IEEE/CVF conference on computer vision and pattern recognition*, pp. 24185–24198, 2024.
- Dong, B., Ni, M., Huang, Z., Yang, G., Zuo, W., and Zhang, L. Mirage: Assessing hallucination in multimodal reasoning chains of mllm. *arXiv preprint arXiv:2505.24238*, 2025.
- Duan, H., Yang, J., Qiao, Y., Fang, X., Chen, L., Liu, Y., Dong, X., Zang, Y., Zhang, P., Wang, J., et al. Vlmevalkit: An open-source toolkit for evaluating large multi-modality models. In *Proceedings of the 32nd ACM international conference on multimedia*, pp. 11198–11201, 2024.
- Fu, X., Hu, Y., Li, B., Feng, Y., Wang, H., Lin, X., Roth, D., Smith, N. A., Ma, W.-C., and Krishna, R. Blink: Multimodal large language models can see but not perceive. In *European Conference on Computer Vision*, pp. 148–166. Springer, 2024.
- Gao, J., Li, Y., Cao, Z., and Li, W. Interleaved-modal chain-of-thought. In *Proceedings of the Computer Vision and Pattern Recognition Conference*, pp. 19520–19529, 2025.
- Grill, J.-B., Strub, F., Althé, F., Tallec, C., Richemond, P., Buchatskaya, E., Doersch, C., Avila Pires, B., Guo, Z., Gheshlaghi Azar, M., et al. Bootstrap your own latent—a new approach to self-supervised learning. *Advances in neural information processing systems*, 33:21271–21284, 2020.
- Gupta, T. and Kembhavi, A. Visual programming: Compositional visual reasoning without training. In *Proceedings of the IEEE/CVF conference on computer vision and pattern recognition*, pp. 14953–14962, 2023.
- Hao, S., Sukhbaatar, S., Su, D., Li, X., Hu, Z., Weston, J., and Tian, Y. Training large language models to reason in a continuous latent space. *arXiv preprint arXiv:2412.06769*, 2024.
- He, K., Chen, X., Xie, S., Li, Y., Dollár, P., and Girshick, R. Masked autoencoders are scalable vision learners. In *Proceedings of the IEEE/CVF conference on computer vision and pattern recognition*, pp. 16000–16009, 2022.
- Hu, E. J., Shen, Y., Wallis, P., Allen-Zhu, Z., Li, Y., Wang, S., Wang, L., Chen, W., et al. Lora: Low-rank adaptation of large language models. *ICLR*, 1(2):3, 2022.
- Huang, W., Jia, B., Zhai, Z., Cao, S., Ye, Z., Zhao, F., Xu, Z., Hu, Y., and Lin, S. Vision-r1: Incentivizing reasoning capability in multimodal large language models. *arXiv preprint arXiv:2503.06749*, 2025.
- Kirillov, A., Mintun, E., Ravi, N., Mao, H., Rolland, C., Gustafson, L., Xiao, T., Whitehead, S., Berg, A. C., Lo, W.-Y., et al. Segment anything. In *Proceedings of the IEEE/CVF international conference on computer vision*, pp. 4015–4026, 2023.
- Li, B., Zhang, Y., Guo, D., Zhang, R., Li, F., Zhang, H., Zhang, K., Zhang, P., Li, Y., Liu, Z., et al. Llava-onevision: Easy visual task transfer. *arXiv preprint arXiv:2408.03326*, 2024.
- Li, B., Sun, X., Liu, J., Wang, Z., Wu, J., Yu, X., Chen, H., Barsoum, E., Chen, M., and Liu, Z. Latent visual reasoning. *arXiv preprint arXiv:2509.24251*, 2025a.
- Li, D., Wu, T., Lin, B., Chen, Z., Zhang, Y., Li, Y., Cheng, M.-M., and Li, X. WOW-seg: A word-free

- open world segmentation model. In *The Fourteenth International Conference on Learning Representations*, 2026. URL <https://openreview.net/forum?id=AyJPSnElbq>.
- Li, K., Shang, C., Karlinsky, L., Feris, R., Darrell, T., and Herzig, R. Latent implicit visual reasoning. *arXiv preprint arXiv:2512.21218*, 2025b.
- Li, Y., Du, Y., Zhou, K., Wang, J., Zhao, W. X., and Wen, J.-R. Evaluating object hallucination in large vision-language models. *arXiv preprint arXiv:2305.10355*, 2023.
- Li, Y., Zhang, Y., Tang, W., Dai, Y., Cheng, M.-M., Li, X., and Yang, J. Visual instruction pretraining for domain-specific foundation models. *arXiv preprint arXiv:2509.17562*, 2025c.
- Liu, H., Li, C., Wu, Q., and Lee, Y. J. Visual instruction tuning. *Advances in neural information processing systems*, 36:34892–34916, 2023.
- Lu, P., Bansal, H., Xia, T., Liu, J., Li, C., Hajishirzi, H., Cheng, H., Chang, K.-W., Galley, M., and Gao, J. Mathvista: Evaluating mathematical reasoning of foundation models in visual contexts. *arXiv preprint arXiv:2310.02255*, 2023.
- Qin, Y., Wei, B., Ge, J., Kallidromitis, K., Fu, S., Darrell, T., and Wang, X. Chain-of-visual-thought: Teaching vlms to see and think better with continuous visual tokens. *arXiv preprint arXiv:2511.19418*, 2025.
- Shao, H., Qian, S., Xiao, H., Song, G., Zong, Z., Wang, L., Liu, Y., and Li, H. Visual cot: Advancing multimodal language models with a comprehensive dataset and benchmark for chain-of-thought reasoning. *Advances in Neural Information Processing Systems*, 37:8612–8642, 2024.
- Su, Y., Zhang, H., Li, S., Liu, N., Liao, J., Pan, J., Liu, Y., Xing, X., Sun, C., Li, C., et al. Patch-as-decodable-token: Towards unified multi-modal vision tasks in mllms. *arXiv preprint arXiv:2510.01954*, 2025.
- Tong, J., Gu, J., Lou, Y., Fan, L., Zou, Y., Wu, Y., Ye, J., and Li, R. Sketch-in-latents: Eliciting unified reasoning in mllms. *arXiv preprint arXiv:2512.16584*, 2025.
- Tong, P., Brown, E., Wu, P., Woo, S., IYER, A. J. V., Akula, S. C., Yang, S., Yang, J., Middepogu, M., Wang, Z., et al. Cambrian-1: A fully open, vision-centric exploration of multimodal llms. *Advances in Neural Information Processing Systems*, 37:87310–87356, 2024.
- Tu, S., Zhang, Q., Sun, J., Fu, Y., Li, L., Lan, X., Jiang, D., Wang, Y., and Zhao, D. Perception-consistency multimodal large language models reasoning via caption-regularized policy optimization. *arXiv preprint arXiv:2509.21854*, 2025.
- Wang, P., Bai, S., Tan, S., Wang, S., Fan, Z., Bai, J., Chen, K., Liu, X., Wang, J., Ge, W., et al. Qwen2-vl: Enhancing vision-language model’s perception of the world at any resolution. *arXiv preprint arXiv:2409.12191*, 2024.
- Wang, Q., Shi, Y., Wang, Y., Zhang, Y., Wan, P., Gai, K., Ying, X., and Wang, Y. Monet: Reasoning in latent visual space beyond images and language. *arXiv preprint arXiv:2511.21395*, 2025a.
- Wang, W., Ding, L., Zeng, M., Zhou, X., Shen, L., Luo, Y., Yu, W., and Tao, D. Divide, conquer and combine: A training-free framework for high-resolution image perception in multimodal large language models. In *Proceedings of the AAAI Conference on Artificial Intelligence*, pp. 7907–7915, 2025b.
- Wu, P. and Xie, S. V?: Guided visual search as a core mechanism in multimodal llms. In *Proceedings of the IEEE/CVF Conference on Computer Vision and Pattern Recognition*, pp. 13084–13094, 2024.
- Wu, P., Zhang, Y., Diao, H., Li, B., Lu, L., and Liu, Z. Visual jigsaw post-training improves mllms. *arXiv preprint arXiv:2509.25190*, 2025a.
- Wu, Q., Yang, X., Zhou, Y., Fang, C., Song, B., Sun, X., and Ji, R. Grounded chain-of-thought for multimodal large language models. *arXiv preprint arXiv:2503.12799*, 2025b.
- Xu, G., Jin, P., Wu, Z., Li, H., Song, Y., Sun, L., and Yuan, L. Llava-cot: Let vision language models reason step-by-step. In *Proceedings of the IEEE/CVF International Conference on Computer Vision*, pp. 2087–2098, 2025.
- Yang, A., Li, A., Yang, B., Zhang, B., Hui, B., Zheng, B., Yu, B., Gao, C., Huang, C., Lv, C., et al. Qwen3 technical report. *arXiv preprint arXiv:2505.09388*, 2025a.
- Yang, L., Kang, B., Huang, Z., Xu, X., Feng, J., and Zhao, H. Depth anything: Unleashing the power of large-scale unlabeled data. In *Proceedings of the IEEE/CVF conference on computer vision and pattern recognition*, pp. 10371–10381, 2024.
- Yang, Z., Yu, X., Chen, D., Shen, M., and Gan, C. Machine mental imagery: Empower multimodal reasoning with latent visual tokens. *arXiv preprint arXiv:2506.17218*, 2025b.

- Zelikman, E., Harik, G., Shao, Y., Jayasiri, V., Haber, N., and Goodman, N. D. Quiet-star: Language models can teach themselves to think before speaking. *arXiv preprint arXiv:2403.09629*, 2024.
- Zhang, H., Wu, W., Li, C., Shang, N., Xia, Y., Huang, Y., Zhang, Y., Dong, L., Zhang, Z., Wang, L., et al. Latent sketchpad: Sketching visual thoughts to elicit multimodal reasoning in mllms. *arXiv preprint arXiv:2510.24514*, 2025a.
- Zhang, J., Xue, L., Song, L., Wang, J., Huang, W., Shu, M., Yan, A., Ma, Z., Niebles, J. C., Savarese, S., et al. Provision: Programmatically scaling vision-centric instruction data for multimodal language models. *arXiv preprint arXiv:2412.07012*, 2024.
- Zhang, R., Zhang, B., Li, Y., Zhang, H., Sun, Z., Gan, Z., Yang, Y., Pang, R., and Yang, Y. Improve vision language model chain-of-thought reasoning. In *Proceedings of the 63rd Annual Meeting of the Association for Computational Linguistics (Volume 1: Long Papers)*, pp. 1631–1662, 2025b.
- Zhang, X., Li, D., Dong, X., Wu, T., Yu, H., Wang, J., Li, Q., and Li, X. Unichange: Unifying change detection with multimodal large language model. *arXiv preprint arXiv:2511.02607*, 2025c.
- Zhang, Z., Zhang, A., Li, M., Zhao, H., Karypis, G., and Smola, A. Multimodal chain-of-thought reasoning in language models. *arXiv preprint arXiv:2302.00923*, 2023.
- Zhao, P., Tian, J., Xing, Q., Zhang, X., Li, Z., Qian, J., Cheng, M.-M., and Li, X. Naipv2: Debaised pairwise learning for efficient paper quality estimation. *arXiv preprint arXiv:2509.25179*, 2025a.
- Zhao, P., Xing, Q., Dou, K., Tian, J., Tai, Y., Yang, J., Cheng, M.-M., and Li, X. From words to worth: Newborn article impact prediction with llm. In *Proceedings of the AAAI Conference on Artificial Intelligence*, volume 39, pp. 1183–1191, 2025b.
- Zheng, Z., Yang, M., Hong, J., Zhao, C., Xu, G., Yang, L., Shen, C., and Yu, X. Deepeyes: Incentivizing” thinking with images” via reinforcement learning. *arXiv preprint arXiv:2505.14362*, 2025.
- Zhou, B., Zhao, H., Puig, X., Fidler, S., Barriuso, A., and Torralba, A. Scene parsing through ade20k dataset. In *Proceedings of the IEEE conference on computer vision and pattern recognition*, pp. 633–641, 2017.
- Zhu, J., Wang, W., Chen, Z., Liu, Z., Ye, S., Gu, L., Tian, H., Duan, Y., Su, W., Shao, J., et al. Internv13: Exploring advanced training and test-time recipes for open-source multimodal models. *arXiv preprint arXiv:2504.10479*, 2025.

## A. Appendix

### A.1. Experiment Details

**Training Datasets.** To ensure a fair comparison and maintain consistency with prior work, we **directly adopt** the training suite established by (Qin et al., 2025) without any additional modification. The dataset comprises vision-centric subsets from LLaVA-OneVision (Li et al., 2024), TallyQA (Acharya et al., 2019), and ADE20K-Depth (Zhou et al., 2017), following the exact configuration described in the original study.

**Training Configurations.** We fine-tune our model using LoRA (Hu et al., 2022) with a rank  $r = 16$  and an alpha  $\alpha = 32$ . The learning rates are set to  $2 \times 10^{-4}$  for LoRA adapters. All experiments are conducted on a workstation equipped with  $4 \times$  NVIDIA A40 GPUs.

**Settings of baselines** We directly obtained the reported results of SKILA and LVR from their respective papers. For **SKILA**, we adopt the Unified Reasoning Model (SKILA) rather than SKILA-V. The results for **LVR** are taken from the experimental reports in the SKILA paper. For **CoVT**, we downloaded the CoVT-seg-dino-depth model and conducted local evaluation following the official setup. For **LIVR**, we follow the training protocol described in the original paper, performing a two-stage training process with 4K steps for each stage.

### A.2. Examples of conversation on different tasks

We provide more question and answer examples in Fig. 7 and Fig. 8.

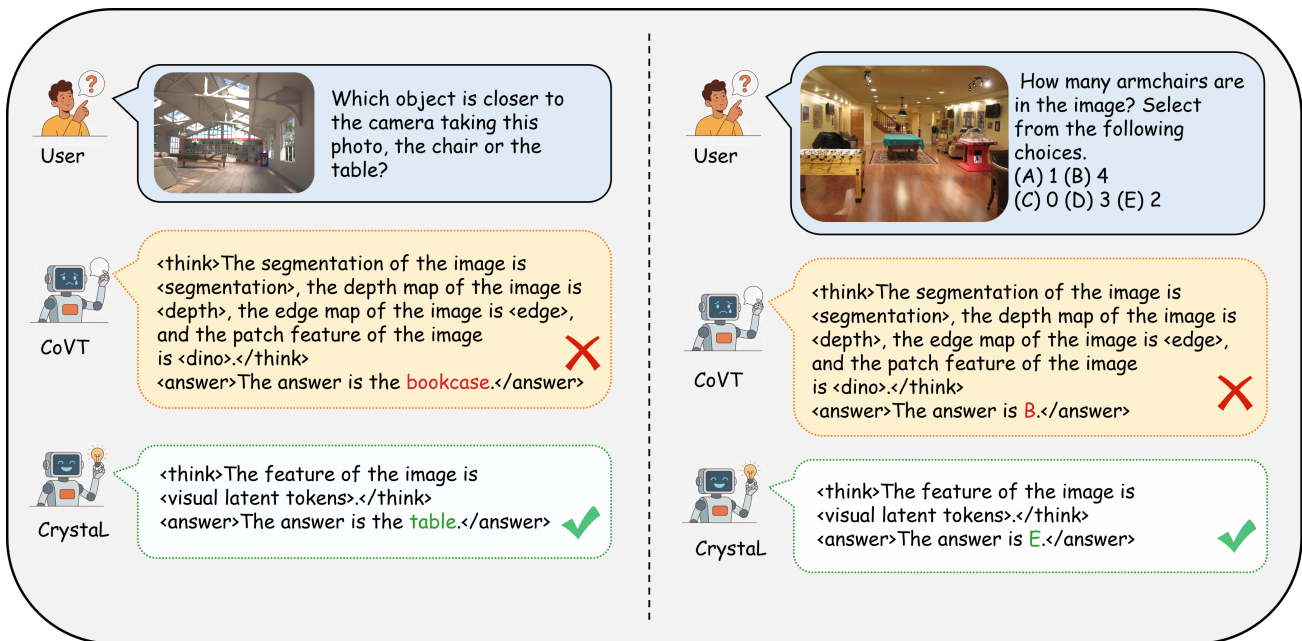


Figure 7. Results on counting and depth

### A.3. Demonstration on corrupted examples

The illustration of five kinds of corruption  $\mathcal{C}$  is in Fig. 9, 10, 12, 11, 13

### A.4. Attention map during training

To analyze how the two paths work, we visualize the attention maps during training in Fig. 14, 15, 16. The left part corresponds to the intact path, while the right one corresponds to the corrupted path.

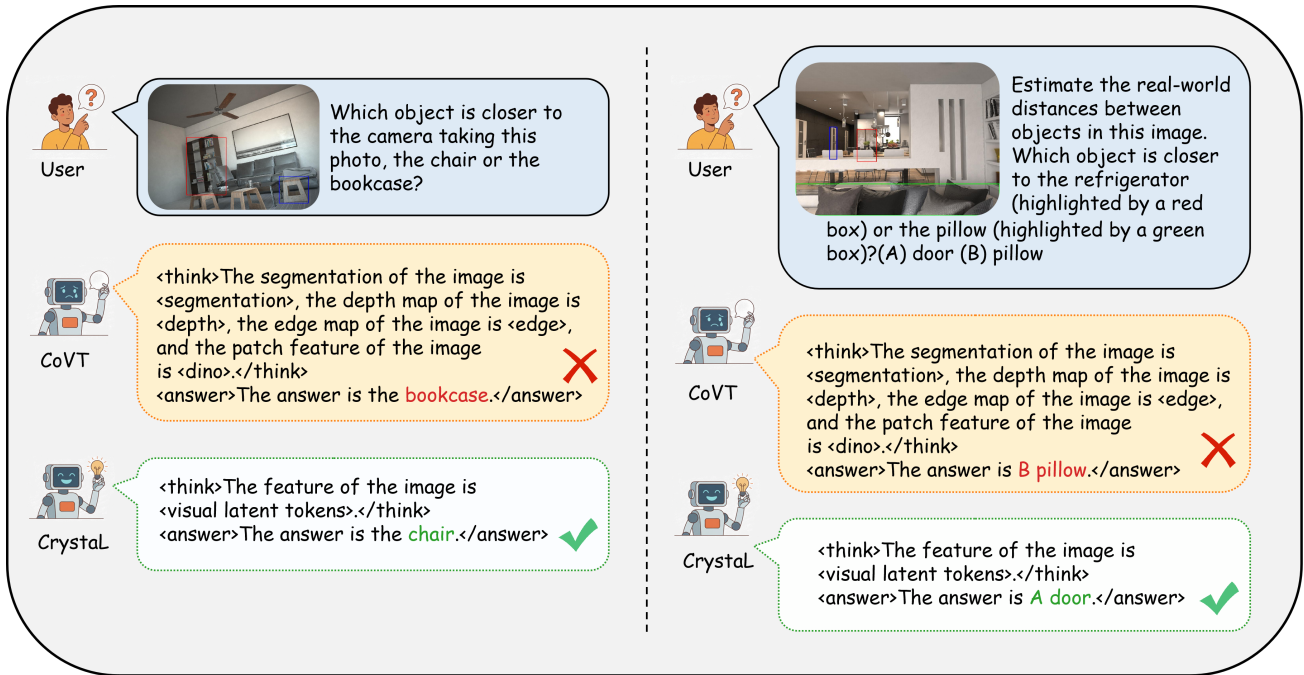


Figure 8. Results on relation and distance.



Figure 9. Gaussian blur variations. We illustrate the multi-scale blurring responses applied to the input samples, showing the original image and three levels of Gaussian smoothing ( $r = 2, 5, 10$ ).

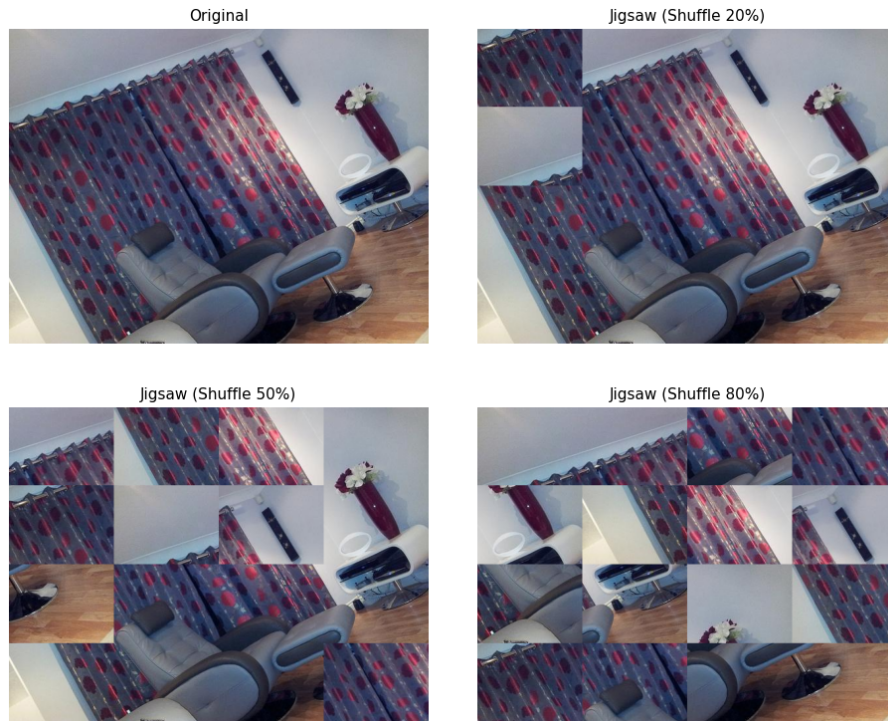


Figure 10. **Jigsaw**. We apply Jigsaw augmentation to the input samples to challenge the model’s ability to capture global structural consistency. Three levels of shuffling ratios ( $\rho \in \{20\%, 50\%, 80\%\}$ ) are illustrated to demonstrate increasing spatial complexity.

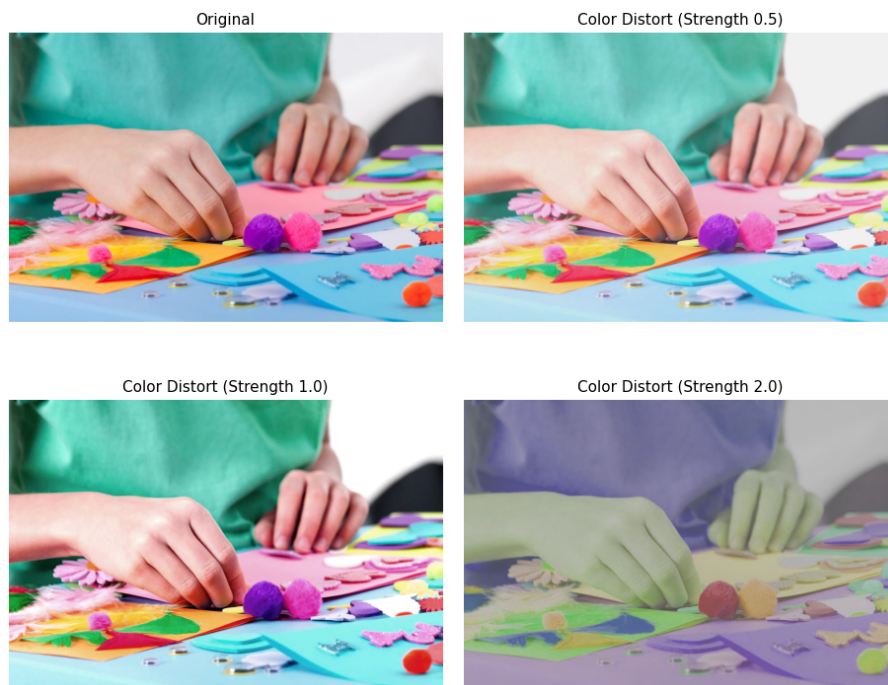


Figure 11. **Colour Distort**. We illustrate the visual variations generated by the color jittering module by modulating brightness, contrast, saturation, and hue with increasing intensities ( $s \in \{0.5, 1.0, 2.0\}$ ).



Figure 12. **Gaussian Noise.** We illustrate the original image and its corrupted versions subjected to additive Gaussian noise with varying standard deviations ( $\sigma \in \{15, 30, 50\}$ ).

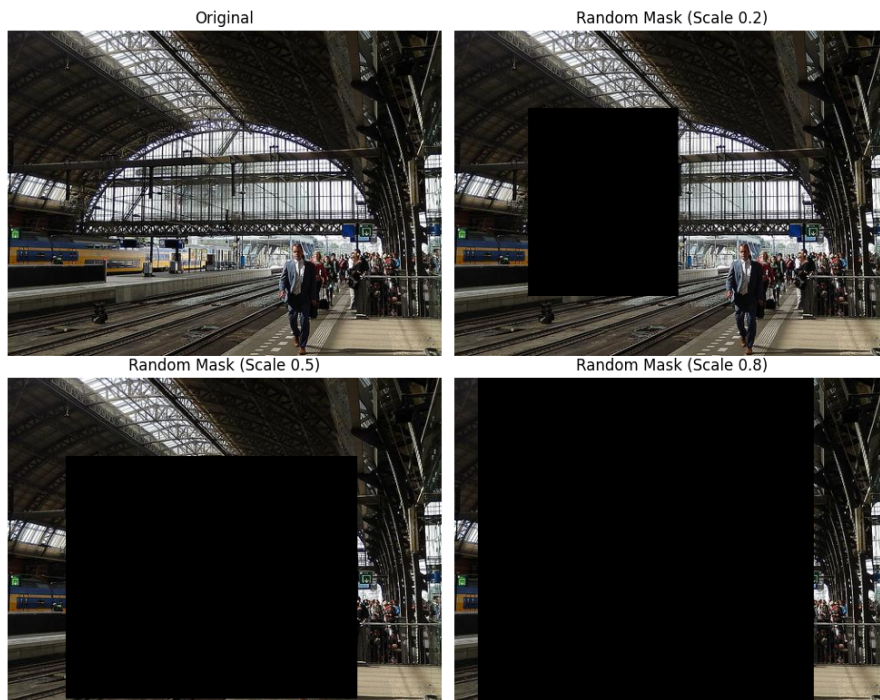


Figure 13. **Random mask.** We demonstrate the original image alongside three variants of Random Erasing at different scales ( $s \in \{0.2, 0.5, 0.8\}$ ).

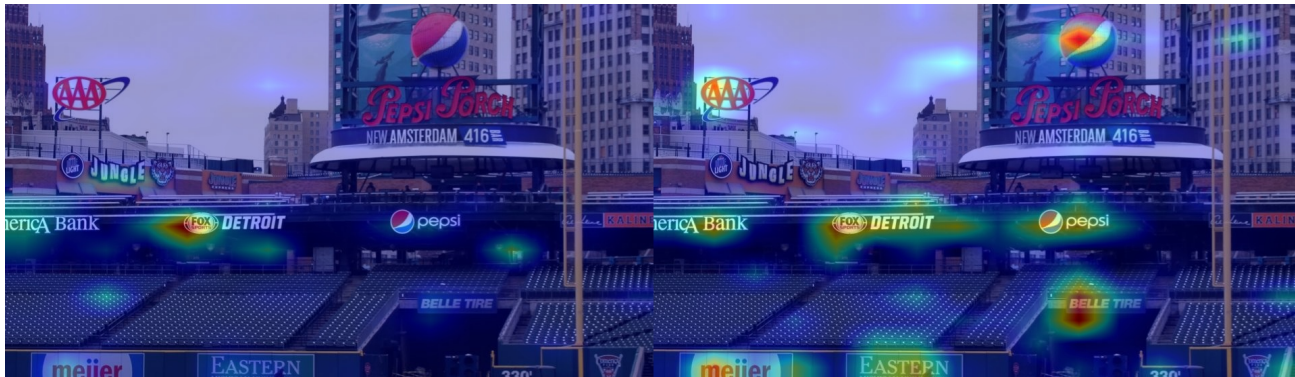


Figure 14. Attention differences. The intact path attends to detroit while the corrupted path attends to all the labels.



Figure 15. Attention differences. The intact path attends to random positions while the corrupted path attends to the text behind the man.

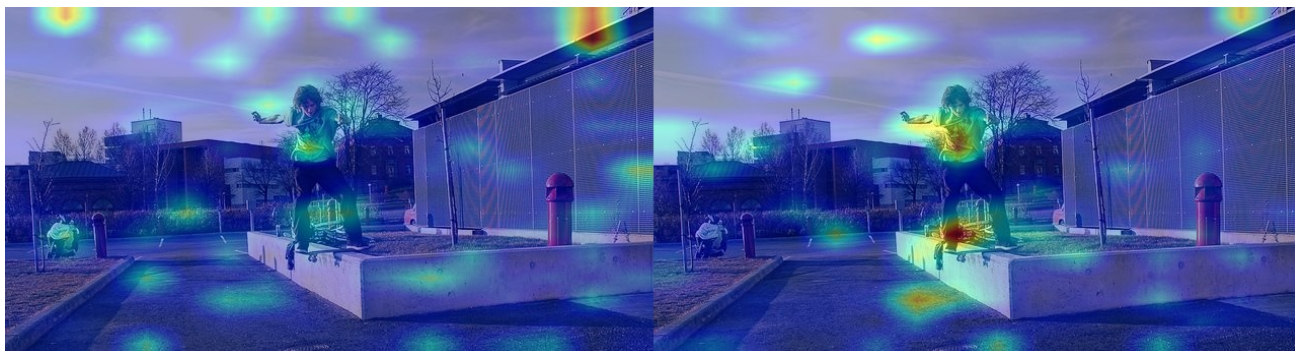


Figure 16. Attention differences. The intact path attends to random positions while the corrupted path attends to the man.